Convergent close-coupling calculations of electron-hydrogen scattering

Igor Bray*
Electronic Structure of Materials Centre, School of Physical Sciences, The Flinders University of South Australia, G.P.O. Box 2100, Adelaide 5001, Australia

Andris T. Stelbovics†
Centre for Atomic, Molecular and Surface Physics, School of Mathematical and Physical Sciences, Murdoch University, Perth 6150, Australia
(Received 6 April 1992)

The convergence of the close-coupling formalism is studied by expanding the target states in an orthogonal L^2 Laguerre basis. The theory is without approximation, and convergence is established by simply increasing the basis size. We present convergent elastic, $2s$, and $2p$ differential cross sections, spin asymmetries, and angular-correlation parameters for the $2p$ excitation at 35, 54.4, and 100 eV. Integrated and total cross sections as well as T-matrix elements for the first five partial waves are also given.

PACS number(s): 34.80.Bm, 34.80.Dp, 34.80.Nz

I. INTRODUCTION

The electron-hydrogen scattering problem is an ideal testing ground for any scattering theory as this is the only electron-atom scattering problem where the target wave functions are known exactly. This relatively simple problem continues to attract considerable interest as there are still significant discrepancies between theory and experiment.

The close-coupling equations for electron-hydrogen scattering, in principle, provide a complete description of the scattering process if they are solved without approximation and if correct three-body boundary conditions are applied to the channels with three free particles in the asymptotic region. They are derived by taking an expansion of the electron-hydrogen atom wave function over the complete set of target states. Because there are an infinite number of discrete and continuum target states, methods must be devised in order to render the equations numerically soluble. One method which suggests itself is to replace the integration over the continuum states of the close-coupling equations by a numerical quadrature. The convergence of such a method can be determined by increasing the order of the quadrature until scattering amplitudes are stable to a specified accuracy, for example 1%. This approach has two drawbacks. Firstly, this quadrature still leaves an infinite sum over the discrete inelastic states of the target which needs further treatment. Secondly, a quadrature formula applied in the most obvious way will use regular Coulomb functions in the calculation of the potentials. Numerical difficulties in calculating integrals involving transitions between continuum channels have made this an unattractive proposition to date.

There is, however, another approach to evaluating the sum over discrete and integral over continuum target states which treats them on an equal footing and is referred to as the pseudostate method. A set of L^2 functions is chosen in which to diagonalize the target Hamiltonian so that the wave functions for the channels over which we calculate T-matrix amplitudes are accurately determined. The remaining states from such a diagonalization have negative and positive eigenenergies. The assumption implicit in this method is that, when the set of functions is carefully selected, as their number increases without limit, they form a basis for the Hilbert space of the target. Thus the expectation is that answers one obtains by solving the coupled-channel equations, when the sum and integral over the true target states are replaced by a discrete sum over the pseudostates, will converge with sufficiently large basis sets.

In terms of testing the basic assumptions of the pseudostate method and understanding its theoretical justification the work of several groups deserves mention. Early numerical calculations for the electron-hydrogen problem utilizing pseudostates were carried out by Burke and Webb [1]. They demonstrated that the inclusion of a few pseudostates significantly reduced the cross sections for scattering, bringing them into better agreement overall with experiment. It was soon realized that with pseudostates one often has the problem that spurious resonance features are introduced into the model cross sections. A study of the convergence properties of pseudostate sets was undertaken by Burke and Mitchell [2]. They considered the model of electron-hydrogen scattering that only treats states of zero orbital angular momentum. Progressing systematically by including more states, they concluded from their study of the singlet $L = 0$ partial wave amplitude that the model calculations were converging except in the neighborhood of the pseudoresonance features. This work while exploring the numerical advantages of pseudostates did not pursue the deeper question of the nature of the quadrature rules that pseudostate target expansions induced, nor did they attempt to establish the relationship between pseudostates and true target continuum states. The pioneer-

ing work in this connection was carried out in a series of papers proposing a method commonly referred to as the J-matrix method of atomic scattering [3]. Through the use of a Laguerre function basis the nature of the quadrature could be explored. The quadrature rules were of a Gaussian type and the underlying orthogonal polynomials were shown by Yamani and Reinhardt [4] to be those of the Pollaczeck class. They were also able to demonstrate the manner in which each pseudostate derived from a finite subset of the Laguerre basis is related to the continuum functions; apart from an overall normalization constant, the pseudostates were the Fourier expansions of the continuum functions truncated to the N-function basis set. The nature of the convergence was studied by Stelbovics and Winata [5], who showed the convergence rate was very slow with the pointwise convergence being of conditional type only.

An important advance in the theory of this model of electron-hydrogen scattering was provided by Poet [6], who solved it using a method which relied on the separable nature of the potential of the three-body Schrödinger equation. The solutions of the differential equation were, as a result, obtainable analytically and the physical three-body scattering wave function could be constructed by matching linear combinations of the solutions to the physical boundary conditions. The resulting equations were simpler than those of the close-coupling formulation and could be solved to a high degree of accuracy. A later comparison by Poet [7] confirmed the earlier conclusions by Burke and co-workers concerning the convergence of the pseudostate method. Further studies involving basis sets comprising Slater functions were undertaken by Oza and Callaway [8, 9] for this model. They considered basis sets of up to nine states and found that pseudoresonance behavior was still present although the size and extent of the pseudothreshold behavior appeared diminished for the largest basis. This conclusion was in the same vein as that deduced earlier by Heller and Yamani [10] in a 10-state J-matrix calculation.

The work described so far left an important question unanswered. Were pseudoresonances a necessary feature of the close-coupling method, which could only be eliminated by some averaging technique as used in [8]? Bray and Stelbovics [11] demonstrated this was not the case. By extending the Laguerre basis size to as many as 30 states, they showed that close-coupling equations yield convergent results at all energies, for scattering and ionization channels, in complete agreement with Poet [6, 7]. This is a most important result as it means that close-coupling equations are valid at all energies, and that pseudoresonances are simply an indication of the lack of convergence in amplitudes as a function of the number of basis states.

With this information we apply the close-coupling formalism using the Laguerre basis states to the full electron-hydrogen problem, i.e., we treat the full set of partial waves. This leads to very-large-scale calculations that require an expansion of the momentum-space method of solution of the close-coupling equations used by McCarthy and Stelbovics [12], upon which this work is based.

In Sec. II we present the close-coupling formalism and address the issue of nonunique solutions. In Sec. III we show how to solve the Lippmann-Schwinger equation minimizing the amount of computational resources necessary for a particular basis set. In Sec. IV we present our results and compare with experiment and other theories, followed by conclusions in Sec. V.

II. THEORY

In this section we give a derivation of the close-coupling equations in operator form, with sufficient boundary conditions to ensure the uniqueness of the T-matrix coupled equations. The derived form carries over directly to the form applicable to finite-basis expansions of the target states.

The Hamiltonian for the nonrelativistic electron-atomic hydrogen scattering problem is given by

$$H = K_1 + v_1 + K_2 + v_2 + v_3, \tag{1}$$

where K_1 and K_2 are, respectively, the projectile- and target-electron kinetic energy operators, and v_1, v_2, and v_3 are the projectile-proton, target-proton, and projectile-target potentials.

The solution of the full Schrödinger equation

$$(E - H)|\Psi^S\rangle = 0 \tag{2}$$

requires the determination of a wave function possessing the symmetry

$$\begin{aligned}\Psi^S(\mathbf{r}_1, \mathbf{r}_2) &= (-1)^S \Psi^S(\mathbf{r}_2, \mathbf{r}_1) \\ &= (-1)^S P_r \Psi^S(\mathbf{r}_1, \mathbf{r}_2),\end{aligned} \tag{3}$$

where S is the total spin and P_r denotes the space exchange operator.

A. Exact target states

In the close-coupling method the wave function (3) is expanded over the complete set, discrete and continuous, of target states $\phi_i(\mathbf{r})$ as

$$\Psi^S(\mathbf{r}_1, \mathbf{r}_2) = \sum\!\!\!\!\!\!\int_i \phi_i(\mathbf{r}_2) f_i^S(\mathbf{r}_1) \tag{4}$$

$$= (-1)^S \sum\!\!\!\!\!\!\int_i \phi_i(\mathbf{r}_1) f_i^S(\mathbf{r}_2). \tag{5}$$

Here the states $\phi_i(\mathbf{r})$ are the exact eigenstates of the target Hamiltonian with

$$(K_2 + v_2)|\phi_i\rangle = \varepsilon_i|\phi_i\rangle. \tag{6}$$

The functions $f_i^S(\mathbf{r})$, by consideration of $\langle\phi_j\phi_k|\Psi^S\rangle$ in (4) and (5), must satisfy

$$\langle\phi_j|f_k^S\rangle = (-1)^S\langle\phi_k|f_j^S\rangle. \tag{7}$$

In standard close-coupling formulations, see Ref. [13] for example, the symmetry condition (3) is imposed by making the expansion (4) manifestly symmetric by writ-

ing

$$\Psi^S(\mathbf{r}_1,\mathbf{r}_2)=\frac{1}{2}\sum\!\!\!\!\!\!\int_i [\,\phi_i(\mathbf{r}_2)F_i^S(\mathbf{r}_1) +(-1)^S\phi_i(\mathbf{r}_1)F_i^S(\mathbf{r}_2)]. \quad (8)$$

However, such an expansion does not lead to a unique solution for the $F_i^S(\mathbf{r})$; if one takes a particular solution of (8) [for example, the $f_i^S(\mathbf{r})$ is one such solution] then so are

$$F_i^S(\mathbf{r})=f_i^S(\mathbf{r})+\sum_j c_{ij}^S\phi_j(\mathbf{r}) \quad (9)$$

for discrete i, and

$$F_i^S(\mathbf{r})=f_i^S(\mathbf{r})+\int_j c_{ij}^S\phi_j(\mathbf{r}) \quad (10)$$

for continuous i, where the arbitrary constants c_{ij}^S satisfy

$$c_{ij}^S+(-1)^S c_{ji}^S=0. \quad (11)$$

Note that the c_{ij}^S are only defined for either i and j both discrete or both continuous.

To avoid this problem of nonunique solutions for $F_i^S(\mathbf{r})$ we impose the condition (7) to the manifold of solutions. It is seen this, in conjunction with (11) selects the solution $F_i^S=f_i^S$. We are now in a position to derive our close-coupling equations. We avoid summation over channel indices throughout by using projections over the complete set of target states labeled in an obvious manner for coordinates of electrons 1 and 2. Defining the identity operators I_1 and I_2 by

$$I_1=\sum\!\!\!\!\!\!\int_i |\ \phi_i\rangle\langle\phi_i\ |, \qquad I_2=\sum\!\!\!\!\!\!\int_i |\phi_i\ \rangle\langle\ \phi_i|, \quad (12)$$

we write the multichannel expansion (4) as

$$|\Psi^S\rangle=I_2|\Psi^S\rangle, \quad (13)$$

and hence

$$P_r|\Psi^S\rangle=I_1P_rI_2|\Psi^S\rangle. \quad (14)$$

Writing $I_2|\Psi^S\rangle$ instead of $|\Psi^S\rangle$ explicitly indicates that the multichannel expansion for the complete wave function is being used. The symmetry condition (7) can then be expressed more usefully as

$$I_2|\Psi^S\rangle=(-1)^SI_1P_rI_2|\Psi^S\rangle. \quad (15)$$

Using (13) we express (2) as

$$\begin{aligned}0&=(E-H)I_2|\Psi^S\rangle\\&=(E-H)\tfrac{1}{2}[1+(-1)^SP_r]I_2|\Psi^S\rangle,\end{aligned} \quad (16)$$

where we introduced the operator $[1+(-1)^SP_r]/2$, which commutes with H, to symmetrize $|\Psi^S\rangle$ numerically. If $|\Psi^S\rangle$ already had the required symmetry then this operator would be redundant. Without the condition (15) it amounts to the explicit symmetrization (8) which yields nonunique solutions.

Using I_2 as a projection operator we write (16) as

$$0=I_2(E-H)[1+(-1)^SP_r]I_2|\Psi^S\rangle \quad (17)$$

which we split to get

$$I_2(E-K_1-K_2-v_2)I_2|\Psi^S\rangle=I_2V^SI_2|\Psi^S\rangle, \quad (18)$$

where

$$V^S=v_1+v_3+(-1)^S(H-E)P_r. \quad (19)$$

We impose condition (15) with the aid of (14) in the E term above,

$$\begin{aligned}(-1)^SEI_2P_rI_2|\Psi^S\rangle&=(-1)^SEI_2I_1I_1P_rI_2|\Psi^S\rangle\\&=EI_1I_2|\Psi^S\rangle\\&=(-1)^SE(1-\theta)I_2P_rI_2|\Psi^S\rangle\\&\quad+E\theta I_1I_2|\Psi^S\rangle,\end{aligned} \quad (20)$$

where θ is an arbitrary constant and incorporates condition (15) for $\theta\neq 0$. So instead of using V^S in (18) we use $V^S(\theta)$ where

$$V^S(\theta)=v_1+v_3-E\theta I_1+(-1)^S[H-E(1-\theta)]P_r. \quad (21)$$

Rather than solving explicitly for the functions $f_i^S(\mathbf{r})$ we form the Lippmann-Schwinger equation for the T matrix

$$T^S=\langle\mathbf{k}\phi|I_2V^S(\theta)I_2|\Psi^{S(+)}\rangle, \quad (22)$$

where $|\mathbf{k}\phi\rangle$ are the asymptotic states satisfying

$$I_2(E-K_1-K_2-v_2)I_2|\mathbf{k}\phi\rangle=0, \quad (23)$$

and where the notation $(+)$ indicates outgoing spherical wave boundary conditions. Combining (18), (22), and (23) the T matrix for the transition of the target in state ϕ_{i_0} to state ϕ_i on impact of projectile $\mathbf{k}_0$ is then given by the Lippmann-Schwinger equation

$$\langle\mathbf{k}\phi_i|T^S|\phi_{i_0}\mathbf{k}_0\rangle=\langle\mathbf{k}\phi_i|V^S(\theta)|\phi_{i_0}\mathbf{k}_0\rangle+\sum\!\!\!\!\!\!\int_{i'}d^3k'\frac{\langle\mathbf{k}\phi_i|V^S(\theta)|\phi_{i'}\mathbf{k}'\rangle\langle\mathbf{k}'\phi_{i'}|T^S|\phi_{i_0}\mathbf{k}_0\rangle}{E-\varepsilon_{i'}-k'^2+i0}. \quad (24)$$

Any nonzero θ will have implemented the symmetry condition (15), and leads to a unique answer independent of θ. So even though the V-matrix elements have an arbitrary constant the solution of the integral equation is independent of this constant. This is confirmed by our numerical investigations.

Previous work done by McCarthy and Stelbovics [12] using momentum-space coupled channel formalism for electron-atom scattering did not employ the symmetry condition (15). This is equivalent to taking $\theta=0$ above. The nonuniqueness manifested itself as instability in the off-the-energy-shell T matrix only, and so did not cause

great concern. Stelbovics [14] has shown analytically that this is indeed the case by studying the nature of the homogeneous solutions of the $\theta = 0$ Lippmann-Schwinger equation (24). He then used this analysis to obtain new V-matrix elements, similar to (21), which yield unique solutions off the energy shell as well. Here we have derived the new form in a simpler way. Even though on-shell amplitudes are unique even if $\theta = 0$, we find that numerical instability occurs when a large number of channels is involved. This problem disappears whenever we introduce a nonzero θ. It has been utilized in all our calculations, where we have taken $\theta = 1/2$.

B. Square-integrable states

In practice no numerical method for solving the coupled T-matrix equations in the form (24) has yet been implemented. The difficulty is the fact that in order to solve this integral equation it must be closed by allowing the index i to run over the same complete range as i', which leads to singular V-matrix elements whenever both i and i' are in the continuum. In principle this is not an insurmountable problem as there is an integral over these elements, but numerically this has proved to be an unattractive option to date.

A number of approximate methods can be applied. The simplest is to truncate the range of i' to some finite set of bound states, thus ignoring the effect of other bound states and the continuum. Unfortunately their effect is important and their omission leads to nonconvergent amplitudes. Alternatively one can use Feschbach formalism to include the effect of the truncated states by adding a complex nonlocal polarization potential which is calculated from the truncated states. The latter has been the major approach of Bray, Konovalov, and McCarthy [15] who have attempted to calculate the polarization potential *ab initio* with fewer and fewer approximations.

The approach that is taken in this work is to diagonalize the hydrogen target Hamiltonian in a set of L^2 functions which when extended to completeness form a basis for the target Hilbert space. The use of L^2 functions eliminates the problem of singular continuum-continuum V-matrix elements. Also most importantly, with a known basis the convergence of the expansions can be studied in a systematic manner with increasing number of basis functions.

We introduce a finite set of N square-integrable states $|\bar{\phi}_i^N\rangle$ which satisfy

$$\langle \bar{\phi}_i^N | K_2 + v_2 | \bar{\phi}_j^N \rangle = \bar{\varepsilon}_i^N \delta_{ij}, \tag{25}$$

and have the property

$$\sum\!\!\!\!\!\!\int_i \phi_i(\mathbf{r}_2) f_i^S(\mathbf{r}_1) = \lim_{N\to\infty} \sum_{i=1}^{N} \bar{\phi}_i^N(\mathbf{r}_2) \bar{f}_i^{SN}(\mathbf{r}_1). \tag{26}$$

With these definitions, the sum and integral in (12) and the Lippmann-Schwinger equation (24) become a single sum over N, with the target states and energies being replaced by $|\bar{\phi}_i^N\rangle$ and $\bar{\varepsilon}_i^N$, respectively. So instead of I_1 and I_2, we define

$$I_1^N = \sum_{i=1}^{N} |\ \bar{\phi}_i^N\rangle\langle\bar{\phi}_i^N\ |, \qquad I_2^N = \sum_{i=1}^{N} |\bar{\phi}_i^N\ \rangle\langle\ \bar{\phi}_i^N|, \tag{27}$$

and have

$$\langle \mathbf{k}\bar{\phi}_i^N | T^{SN} | \bar{\phi}_{i_0}^N \mathbf{k}_0 \rangle = \langle \mathbf{k}\bar{\phi}_i^N | V^{SN}(\theta) | \bar{\phi}_{i_0}^N \mathbf{k}_0 \rangle + \sum_{i'=1}^{N} \int d^3k' \frac{\langle \mathbf{k}\bar{\phi}_i^N | V^{SN}(\theta) | \bar{\phi}_{i'}^N \mathbf{k}' \rangle \langle \mathbf{k}'\bar{\phi}_{i'}^N | T^{SN} | \bar{\phi}_{i_0}^N \mathbf{k}_0 \rangle}{E - \bar{\varepsilon}_{i'} - k'^2 + i0}, \tag{28}$$

where for the physical T-matrix elements of interest we must have $|\phi_i\rangle = |\bar{\phi}_i^N\rangle$ and $|\phi_{i_0}\rangle = |\bar{\phi}_{i_0}^N\rangle$ to sufficiently high precision. With these definitions we have

$$\langle \mathbf{k}\phi_i | T^S | \phi_{i_0} \mathbf{k}_0 \rangle = \lim_{N\to\infty} \langle \mathbf{k}\bar{\phi}_i^N | T^{SN} | \bar{\phi}_{i_0}^N \mathbf{k}_0 \rangle \tag{29}$$

for the physical T-matrix elements. The projection operator I_1 is replaced by I_1^N in calculating the matrix elements of $V^{SN}(\theta)$ in (21), and I_2 is replaced by I_2^N in (23) which yields the $\bar{\varepsilon}_{i'}^N$ energies in the Green's function of (28).

The states $|\bar{\phi}_i^N\rangle$ are obtained by diagonalizing the target Hamiltonian (25), for each l of the target electron, in the Laguerre basis $\xi_{kl}(r)$ which has the form

$$\xi_{kl}(r) = \left(\frac{\lambda(k-1)!}{(2l+1+k)!}\right)^{1/2} (\lambda r)^{l+1} \times \exp(-\lambda r/2) L_{k-1}^{2l+2}(\lambda r), \tag{30}$$

where the $L_{k-1}^{2l+2}(\lambda r)$ are the associated Laguerre polynomials, and k ranges from 1 to the basis size N_l. The constant λ is arbitrary and is chosen so that the lowest energy states are essentially the exact hydrogen eigenstates. For convenience take $\lambda = 2$ for all l. This gives the exact $1s$ state from the diagonalization for $N_0 \geq 1$. The rate of convergence to other exact hydrogen bound states for this λ as a function of N_l has been given by Bray, Konovalov, and McCarthy [15]. We have established that convergence is independent of the value of λ in [11], though the rate of convergence would certainly be affected by choosing an inappropriate value.

This choice of basis we consider to be very important. Unlike the Slater basis, the Laguerre basis is orthogonal, and so does not suffer from any linear dependence problems as the basis size is increased. With this basis we are able to obtain as many as 100 orthonormal states upon diagonalization of the Hamiltonian for each l. Thus, this basis is ideal for convergence studies. Furthermore, the nature of the quadrature in (26) has been studied in detail by a number of authors, see Refs. [4,16,17] for example. It is a Gaussian-type quadrature and the underlying orthogonal polynomials are of the Pollaczeck class. It

can be shown that the weights of the negative energy L^2 states converge to unity in Eq. (26) in the limit of large N and that $\lim_{N\to\infty}\bar{\phi}_i^N = \phi_i$, $\lim_{N\to\infty}\bar{f}_i^{SN} = f_i^S$. This ensures that the limiting procedure (29) gives the correct T-matrix amplitudes (24) for the transitions to the $1s$, $2s$, and $2p$ levels. We also mention for completeness (although it has no bearing on the calculations reported here) that the positive energy L^2 states cannot converge to the non-L^2 regular Coulomb functions. It can be shown [4, 5] that the Gaussian weight function together with the positive-energy weights in the quadrature (26) define a renormalization of the L^2 states so that they approximate the true continuum functions for the first few oscillations in coordinate space at each positive pseudostate energy. A proper consideration of such normalizations would be required if one was to use the L^2 approximated T-matrix equations to model differential ionization cross sections.

III. SOLUTION OF THE LIPPMANN-SCHWINGER EQUATION

We shall omit the bars as well as explicit N_l dependence in the V-matrix elements to simplify the notation. Subsequent discussion refers only to the L^2 states, and there should be no confusion with the exact target eigenstates.

The partial wave Lippmann-Schwinger equation corresponding to (28) for the reduced T-matrix elements is

$$\langle Lk_{nl}ln \,||\, T^{SJ} \,||\, n_0l_0k_0L_0\rangle = \langle Lk_{nl}ln \,||\, V^{SJ}(\theta) \,||\, n_0l_0k_0L_0\rangle + \sum_{n',l',L'}\int_0^\infty dk'k'^2 \frac{\langle Lk_{nl}ln \,||\, V^{SJ}(\theta) \,||\, n'l'k'L'\rangle}{E-\varepsilon_{n'l'}-k'^2/2+i0}\langle L'k'l'n' \,||\, T^{SJ} \,||\, n_0l_0k_0L_0\rangle, \quad (31)$$

where the projectile is denoted by linear momentum k and orbital momentum L, while the target state is denoted by principal quantum number n and orbital angular momentum l. The total orbital angular momentum is denoted by J, and

$$E = \varepsilon_{n_0l_0} + k_0^2/2 = \varepsilon_{nl} + k_{nl}^2/2 \quad (32)$$

is the on-shell energy. The V-matrix elements are evaluated using (21).

It is our aim to perform very large multichannel calculations so it is important to reduce the amount of computer resources necessary to solve (31). Instead of solving (31) directly, which involves complex T-matrix elements, we rewrite it as

$$\langle Lk_{nl}ln \,||\, T^{SJ} \,||\, n_0l_0k_0L_0\rangle = \langle Lk_{nl}ln \,||\, V^{SJ}(\theta) \,||\, n_0l_0k_0L_0\rangle + \sum_{l',L'}\left[\sum_{n'=1}^{N_{l'}}\mathrm{P}\int_0^\infty dk'k'^2\frac{\langle Lk_{nl}ln \,||\, V^{SJ}(\theta) \,||\, n'l'k'L'\rangle}{E-\varepsilon_{n'l'}-k'^2/2}\langle L'k'l'n' \,||\, T^{SJ} \,||\, n_0l_0k_0L_0\rangle - i\pi\sum_{n'=1}^{N_{l'}^o}k_{n'l'}\langle Lk_{nl}ln \,||\, V^{SJ}(\theta) \,||\, n'l'k_{n'l'}L'\rangle\langle L'k_{n'l'}l'n' \,||\, T^{SJ} \,||\, n_0l_0k_0L_0\rangle\right], \quad (33)$$

where the symbol P indicates that the integral is of the principal value type, and $k_{n'l'}$ is defined for $1 \le n' \le N_{l'}^o \le N_{l'}$ for which

$$k_{n'l'} = \sqrt{2(E-\varepsilon_{n'l'})} \quad (34)$$

is real. In this case we say that the channel $n'l'$ is open (there are $N_{l'}^o$ of these), and if $E < \varepsilon_{n'l'}$ we say that this channel is closed. We can use purely real arithmetic if we introduce the K-matrix formulation by letting

$$\langle Lk_{nl}ln \,||\, K^{SJ} \,||\, n_0l_0k_0L_0\rangle = \sum_{l',L'}\sum_{n'=1}^{N_{l'}^o}\langle Lk_{nl}ln \,||\, T^{SJ} \,||\, n'l'k_{n'l'}L'\rangle \times\left(\delta_{l'l_0}\delta_{L'L_0}\delta_{n'n_0} + i\pi k_{n'l'}\langle L'k_{n'l'}l'n' \,||\, K^{SJ} \,||\, n_0l_0k_0L_0\rangle\right). \quad (35)$$

With this definition (33) becomes

$$\langle Lk_{nl}ln \,||\, K^{SJ} \,||\, n_0l_0k_0L_0\rangle = \langle Lk_{nl}ln \,||\, V^{SJ}(\theta) \,||\, n_0l_0k_0L_0\rangle + \sum_{l',L'}\sum_{n'=1}^{N_{l'}}\mathrm{P}\int_0^\infty dk'k'^2\frac{\langle Lk_{nl}ln \,||\, V^{SJ}(\theta) \,||\, n'l'k'L'\rangle}{E-\varepsilon_{n'l'}-k'^2/2}\langle L'k'l'n' \,||\, K^{SJ} \,||\, n_0l_0k_0L_0\rangle \quad (36)$$

which is solved for the K matrix using real arithmetic, and the T matrix is obtained by solving the much smaller set of equations (35).

There are a number of methods for calculating principal value type integrals. McCarthy and Stelbovics [12] used an on-shell subtraction to remove the singularity, and so they used a single quadrature rule to represent the integral over k' in (36). This method does not work very well when there is a large number of channels. This is due to the fact that as the singularity is different for each $n'l'$ one of the quadrature points often falls near the singularity resulting in a very large subtraction which loses precision. We get around this difficulty by choosing a different quadrature rule for each $n'l'$. Furthermore, rather than using a subtraction, we simply ensure that for each open channel $n'l'$ the singularity is exactly in the middle of an interval which contains an even number of Gaussian points. Thus, for some arbitrary function F we write

$$\mathrm{P}\int_0^\infty dk'k'^2\frac{F(k')}{E-\varepsilon_{n'l'}-k'^2/2}\approx\sum_{j=1}^{N_{n'l'}}w_j^{n'l'}F(k_j^{n'l'}) \tag{37}$$

where the weights $w_j^{n'l'}$ contain Gaussian-type weights as well as the Green's function. In practice we take $N_{n'l'}$ to be the same for each channel $n'l'$. In our calculations our largest Laguerre basis size has $N_l = 13$ (see next section), in which case we find that we require the number of quadrature points $N_{n'l'}$ to be as big as 55. It is generally the case that the larger the basis size the more quadrature points are necessary. This is unfortunate as it means that the size of the matrices grows more rapidly than would be the case if only the basis size was increased. To determine approximately how many quadrature points are necessary we check that the identity

$$1=\int_0^\infty dk'\langle\bar{\phi}_{n'l'}|k'\rangle\langle k'|\bar{\phi}_{n'l'}\rangle \tag{38}$$

is satisfied for each $n' = 1$ to Laguerre basis size $N_{l'}$ to three significant figures.

Denoting the combinations of $Lk_{nl}ln$ by f, $L_0k_0l_0n_0$ by i, and $L'k'l'n'$ by n we write (36) as

$$K_{fi}^{SJ}=V_{fi}^{SJ}(\theta)+\sum_n w_nV_{fn}^{SJ}(\theta)K_{ni}^{SJ}, \tag{39}$$

where the single sum over n contains the sum over $N_{n'l'}$ quadrature points $k_j^{n'l'}$ in (37), and the single index on w_n indicates the complete range of $w_j^{n'l'}$. To solve this equation we form a closed set of linear equations by letting f run over the same range as n. We replace f by n' to indicate this and have

$$\begin{aligned}V_{n'i}^{SJ}(\theta)&=\sum_n\left[\delta_{n'n}-w_nV_{n'n}^{SJ}(\theta)\right]K_{ni}^{SJ}\\&=\sum_n\left[\delta_{n'n}/w_n-V_{n'n}^{SJ}(\theta)\right]w_nK_{ni}^{SJ}.\end{aligned} \tag{40}$$

As both $\delta_{n'n}/w_n$ and $V_{n'n}^{SJ}(\theta)$ are symmetric on interchange of n and n' we need to solve the linear system of the form $AX = B$, where A is a real symmetric matrix. We do this using LAPACK routines [18] that store A in compact form. This way we use the minimal amount of storage space. The usage of real arithmetic and symmetric matrices reduces the storage by a factor of 4. This is invaluable as for our 70-channel calculations (see below), the matrix A occupies $\approx$ 30M of storage $[(55\times70)^2\times4/2]$, where 4 is the number of bytes required to store a real number, and we divide by two since the symmetric matrix is stored in compact form. This allows the linear system to be solved in the core memory of our IBM RS6000/540 computer which has 64M of core memory. Storage of the direct (no S dependence) and exchange (have S dependence) V-matrix elements (21), also real and symmetric, adds a further 60M of required storage space.

The required K_{fi}^{SJ} are calculated by direct substitution of the solution of (40) for the K_{ni}^{SJ} into (39). Having calculated the K_{fi}^{SJ} we recover the T_{fi}^{SJ} by solving (35) which in the simplified notation we write as

$$K_{fi}^{SJ}=\sum_{f'}T_{ff'}^{SJ}\left(\delta_{f'i}+i\pi k_{f'}K_{f'i}^{SJ}\right). \tag{41}$$

Note that the sum in (39) contains all channels, open and closed, as well as the quadrature points, whereas the sum in (41) contains only the open channels.

This procedure is carried out for each value of S ($S = 0$ for singlet, $S = 1$ for triplet) of partial wave J, with as many partial waves taken as necessary for convergence to better than 1%. Typically, we take $J = 0$ to 80 with higher partial waves taken care of by either an extrapolation or by analytic Born subtraction as discussed by McCarthy and Stelbovics [12].

The relation between the reduced T-matrix elements and various physical observables may be found in Refs. [12, 19]. For completeness, we present the definitions of the calculated observables here. Writing the amplitude for the excitation of the $2p$ $m_l = n$ ($n = -1, 0, 1$) substate as a_n, the λ, R, and I parameters are given by

$$\begin{aligned}&\lambda\equiv\langle a_0a_0\rangle/\sigma_{2p},\quad R\equiv\mathrm{Re}\langle a_0a_1\rangle/\sigma_{2p},\\&I\equiv\mathrm{Im}\langle a_0a_1\rangle/\sigma_{2p}=-L_\perp/\sqrt{8},\end{aligned} \tag{42}$$

where σ_{2p} is the differential cross section, the notation $\langle\,\rangle$ indicates a spin weighted sum, and $L_\perp$ is the angular momentum transferred perpendicular to the scattering plane (see review of Anderson, Gallagher, and Hertel [20]). The spin asymmetry A_{nl} for the nl channel is related to the ratio of triplet to singlet scattering for that channel r_{nl} by

$$A_{nl}=\frac{1-r_{nl}}{1+3r_{nl}}. \tag{43}$$

The relationship between the I and $L_\perp$ parameters is particularly worth noting given the remarkable quantitative agreement between experiment and the coupled-channel optical (CCO) theory of Bray and McCarthy [21] in electron-sodium scattering for this and other parameters. This agreement is found for singlet, triplet, and averaged spin states. As the CCO theory [21] is an approximation to the CC theory presented here we also expect excellent quantitative agreement with such parameters in the simpler case of electron-hydrogen scattering. Unfortunately, this does not prove to be the case.

IV. RESULTS

The major discrepancy between theory and experiment for electron-hydrogen scattering is for angular correlation parameters λ and R of the $2p$ excitation. So we apply our theory to those energies where there are most measurements of these parameters namely at 35 and 54.4 eV. We also look at the higher energy of 100 eV to get a broad energy spectrum.

Our aim is to present a series of large basis close-coupling calculations which demonstrate convergence of the close-coupling approach. In the partial wave solution of the close-coupling equations discussed above, convergence with target states, denoted by nl, must be demonstrated separately for n and l.

In Figs. 1–9 the three left-hand pictures have target states with $l_{\max} = 2$, and examine the convergence as N_l is increased for each l ($n = l + 1$ to N_l). The largest N_l, which we take to be the same for each l, that our local computers can handle for this $l_{\max}$ is 13, i.e., $13s$, $12p$, and $11d$ states. This leads to a 70-channel calculation as for $J \geq l_{\max}$ an s state leads to a single channel, a p state generates 2 channels, and a d state generates 3 channels. These calculations are denoted by 70CC. In the three center pictures convergence is examined for fixed N_l, but with increasing l up to and including f states, i.e., $l_{\max} = 3$. The largest calculation that we could perform which had f states has $N_l = 10$ for each l, i.e., $10s$, $9p$, $8d$, and $7f$ states. This leads to an 80-channel (80CC) calculation for $J \geq 3$. Note that even though the 80CC calculation has 10 more channels than the former, it has a total of 34 states, while the 70CC treats 36 states. The three right-hand pictures compare our results with some other theories and if available, experiment. We do not present our quantitative results as they are extremely extensive but they may be readily obtained by corresponding with the authors.

In Fig. 1 we look at the differential cross sections for the $1s$, $2s$, and $2p$ channels at 35 eV. We find excellent convergence as a function of both N_l and $l_{\max}$ for all channels. The convergence is excellent at all angles perhaps with the exception of the very backward angles. There is good agreement with other nonperturbative theories, the coupled-channel optical model (6CCO) of Bray, Konovalov, and McCarthy [19] and the intermediate energy R-matrix method (IERM) of Scholz *et al.* [22]. The exact second-order theory (DWB2) of Madison, Bray, and McCarthy [23] is a little above the other theories, but as it is a perturbative theory we do not expect it to have converged at this relatively low energy.

Figure 2 looks at the convergence in the spin asymmetries (43) at 35 eV. We see that for these parameters the convergence is again very good, but is not quite as rapid as for the differential cross sections. Convergence at the very backward angles for the $2p$ channel has not been achieved which is probably due to the difficulty associated with getting a convergent ratio of differential cross sections where they are very small. Comparison with other theories shows quite a bit of variation. There is considerable agreement with the IERM theory and to a lesser extent with the 6CCO theory. The DWB2 results have quite a different quality at the intermediate angles for the $2s$ and $2p$ channels.

In Fig. 3 we look at the angular correlation parameters, for which there is an extensive set of measurements. Once again we see that convergence as a function of N_l is

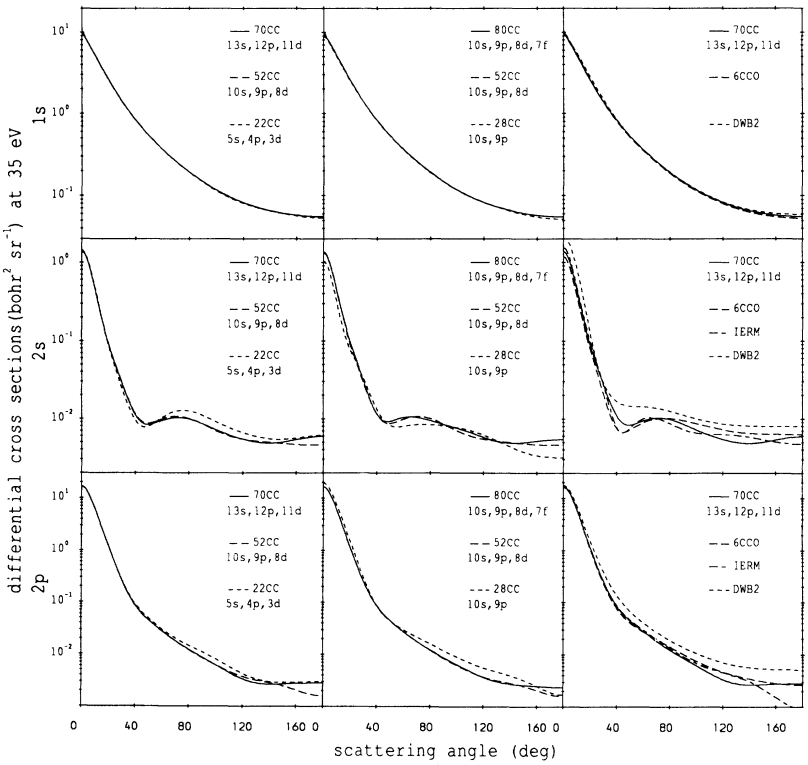

FIG. 1. Differential cross sections at 35 eV for the $1s$, $2s$, and $2p$ channels calculated with the indicated number of Laguerre basis states. The left-hand column has calculations which include d states, so convergence is examined as the basis size is increased for each l. The center column fixes the basis size for each l, and demonstrates convergence as l is increased from s and p states to d and f states. The right-hand column compares the 70CC calculation with other theories. The coupled-channel optical calculation of Bray, Konovalov, and McCarthy [19], intermediate energy R-matrix method of Scholz *et al.* [22], and the distorted-wave second-order Born calculation of Madison, Bray, and McCarthy [23] are denoted by 6CCO, IERM, and DWB2, respectively. Quantitative results may be obtained by corresponding with the authors.

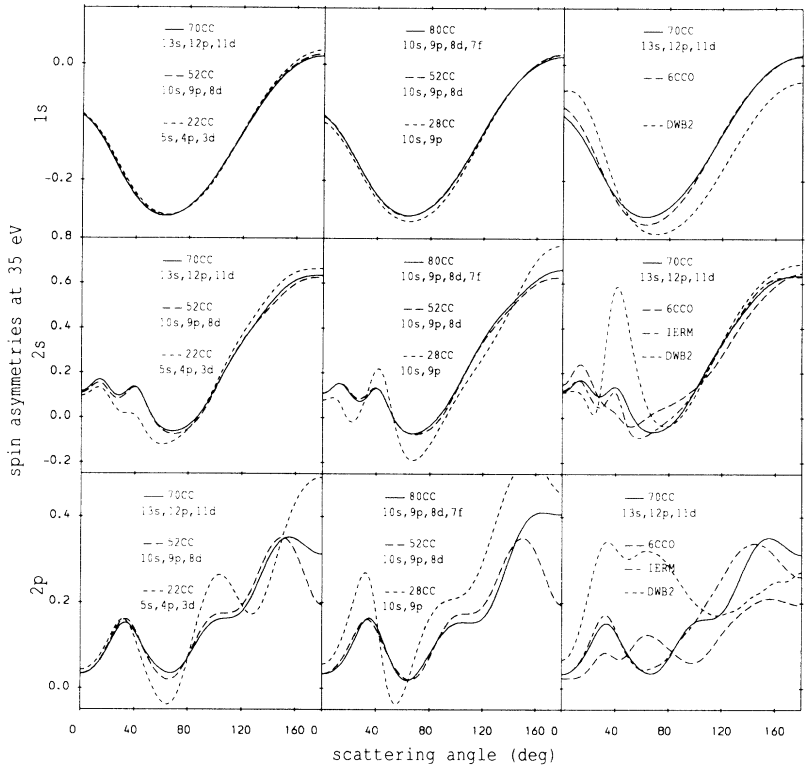

FIG. 2. Spin asymmetries at 35 eV for the $1s$, $2s$, and $2p$ channels calculated with the indicated number of Laguerre basis states. See Fig. 1 for more detail and definition of other theories.

very good. The convergence as a function of l_{max} is very good for most angles except perhaps in the neighborhood of 120°. It is therefore very surprising to find the very large discrepancy between all theories and experiment at the forward angles for the R parameter. Here convergence of the close-coupling results is clearly established, and furthermore, they are in complete agreement with the other theories. Agreement with experiment at other angles is much better, but why this should be the case where the count rate is much smaller, is a mystery. The λ parameter seems to have the opposite behavior. Agreement with theory is very good at forward angles, but gets

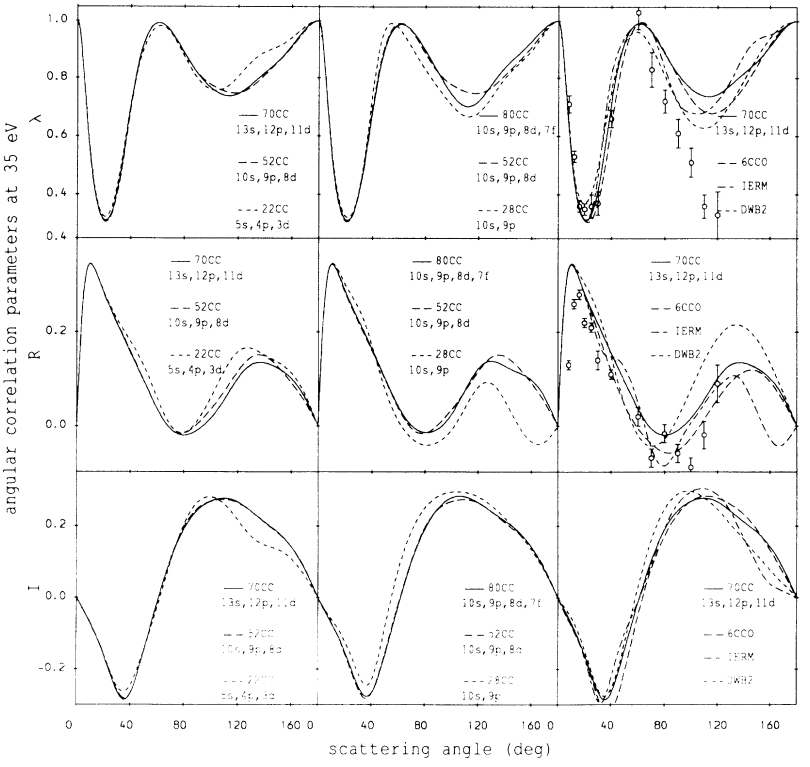

FIG. 3. Angular correlation parameters for the $2p$ excitation of hydrogen at 35 eV calculated with the indicated number of Laguerre basis states. See Fig. 1 for more detail and definition of other theories. The measurements are due to Slevin *et al.* [26].

to be very poor at intermediate to backward angles.

Having looked at pictorial results it is instructive to examine the actual T-matrix elements for the most significant partial waves, as well as the integrated and total cross sections. In Table I we present the 35-eV T-matrix elements for the 52CC, 70CC, and 80CC calculations, and compare them with the IERM results. We also give the integrated $1s$, $2s$, $2p$, and total cross sections, which show convergence and good agreement with IERM. The IERM T_R-matrix elements [22] are related to our T-matrix elements by

$$T_R = -2\pi i\sqrt{k_f k_i}T, \tag{44}$$

where k_f and k_i are the final and incident linear momenta of the projectile. The difference in the 70CC and 80CC results gives a good indication of the convergence, since the two calculations not only treat each partial wave with a different number of states, but also treat a different number of partial waves. If the 70CC and 80CC calcu-

TABLE I. T-matrix elements (real and imaginary parts) for the first five partial waves J, and integrated and total cross sections (in units of a_0^2) at 35 eV. The numbers in brackets indicate powers of 10.

J	S	Channel	52CC	70CC	80CC	IERM
0	0	$1s$-$1s$	-6.74[-2]-8.37[-2]	-6.86[-2]-8.26[-2]	-6.75[-2]-8.39[-2]	
		$1s$-$2s$	-1.19[-2] 1.83[-2]	-1.24[-2] 1.78[-2]	-1.28[-2] 1.87[-2]	-1.36[-2] 1.65[-2]
		$1s$-$2p$	1.31[-2] 2.73[-2]	1.16[-2] 2.79[-2]	1.21[-2] 2.73[-2]	1.32[-2] 2.94[-2]
	1	$1s$-$1s$	-8.63[-2]-1.41[-1]	-8.61[-2]-1.41[-1]	-8.63[-2]-1.41[-1]	
		$1s$-$2s$	-1.09[-2] 2.46[-3]	-1.03[-2] 1.95[-3]	-1.09[-2] 2.34[-3]	-1.03[-2] 1.19[-3]
		$1s$-$2p$	-6.18[-3] 1.71[-2]	-6.11[-3] 1.72[-2]	-6.40[-3] 1.71[-2]	-6.79[-3] 1.73[-2]
1	0	$1s$-$1s$	-2.24[-2]-2.01[-2]	-2.24[-2]-2.00[-2]	-2.25[-2]-2.01[-2]	
		$1s$-$2s$	1.51[-2] 1.73[-2]	1.51[-2] 1.78[-2]	1.52[-2] 1.78[-2]	1.45[-2] 1.73[-2]
		$1s$-$2p_-$	1.07[-2] 1.24[-2]	1.06[-2] 1.28[-2]	1.07[-2] 1.24[-2]	1.17[-2] 1.32[-2]
		$1s$-$2p_+$	1.14[-2]-1.54[-4]	1.15[-2] 2.72[-4]	1.14[-2]-4.96[-4]	1.26[-2] 5.12[-4]
	1	$1s$-$1s$	-6.83[-2]-3.14[-2]	-6.87[-2]-3.17[-2]	-6.84[-2]-3.14[-2]	
		$1s$-$2s$	3.90[-3] 1.40[-2]	3.69[-3] 1.39[-2]	3.81[-3] 1.41[-2]	3.46[-3] 1.36[-2]
		$1s$-$2p_-$	-4.64[-4] 3.50[-3]	-3.67[-4] 3.66[-3]	-5.01[-4] 3.55[-3]	1.08[-4] 4.02[-3]
		$1s$-$2p_+$	6.48[-3] 6.06[-3]	6.68[-3] 6.30[-3]	6.61[-3] 6.06[-3]	7.31[-3] 6.93[-3]
2	0	$1s$-$1s$	-1.43[-2]-1.79[-2]	-1.46[-2]-1.76[-2]	-1.44[-2]-1.79[-2]	
		$1s$-$2s$	6.51[-3] 3.93[-3]	6.39[-3] 4.05[-3]	6.54[-3] 4.03[-3]	5.38[-3] 3.36[-3]
		$1s$-$2p_-$	2.38[-2] 1.07[-2]	2.36[-2] 1.14[-2]	2.38[-2] 1.12[-2]	2.53[-2] 1.17[-2]
		$1s$-$2p_+$	-1.02[-3]-2.76[-3]	-4.69[-4]-2.53[-3]	-4.79[-4]-2.80[-3]	2.56[-4]-3.40[-3]
	1	$1s$-$1s$	-2.70[-2]-7.31[-3]	-2.72[-2]-7.36[-3]	-2.71[-2]-7.32[-3]	
		$1s$-$2s$	9.31[-3] 7.37[-3]	9.19[-3] 7.37[-3]	9.31[-3] 7.44[-3]	8.64[-3] 6.97[-3]
		$1s$-$2p_-$	6.96[-3] 1.07[-2]	6.96[-3] 1.08[-2]	6.92[-3] 1.08[-2]	7.53[-3] 1.11[-2]
		$1s$-$2p_+$	4.21[-3]-1.22[-3]	4.27[-3]-1.06[-3]	4.24[-3]-1.30[-3]	5.60[-3]-1.03[-3]
3	0	$1s$-$1s$	-1.10[-2]-1.01[-2]	-1.12[-2]-9.92[-3]	-1.10[-2]-1.01[-2]	
		$1s$-$2s$	1.00[-3] 4.67[-3]	1.11[-3] 4.76[-3]	1.18[-3] 4.58[-3]	1.56[-4] 4.60[-3]
		$1s$-$2p_-$	2.45[-2] 2.42[-3]	2.41[-2] 2.43[-3]	2.45[-2] 2.71[-3]	2.43[-2] 2.71[-3]
		$1s$-$2p_+$	-3.07[-3] 2.14[-5]	-3.00[-3]-1.57[-4]	-3.03[-3]-1.58[-4]	-2.92[-3] 8.86[-4]
	1	$1s$-$1s$	-1.20[-2]-4.90[-3]	-1.21[-2]-4.94[-3]	-1.21[-2]-4.88[-3]	
		$1s$-$2s$	5.44[-3] 2.75[-3]	5.32[-3] 2.72[-3]	5.38[-3] 2.81[-3]	4.35[-3] 2.50[-3]
		$1s$-$2p_-$	1.57[-2] 1.00[-2]	1.58[-2] 1.01[-2]	1.56[-2] 1.02[-2]	1.62[-2] 1.03[-2]
		$1s$-$2p_+$	2.08[-4]-2.14[-3]	3.09[-4]-2.21[-3]	1.56[-4]-2.12[-3]	3.92[-4]-2.15[-3]
4	0	$1s$-$1s$	-7.45[-3]-5.12[-3]	-7.50[-3]-5.16[-3]	-7.37[-3]-4.98[-3]	
		$1s$-$2s$	2.30[-4] 4.96[-3]	-1.89[-5] 5.08[-3]	3.27[-4] 4.76[-3]	-3.30[-4] 5.39[-3]
		$1s$-$2p_-$	1.98[-2]-5.79[-4]	1.97[-2]-4.50[-4]	1.98[-2] 2.92[-4]	1.97[-2]-4.84[-4]
		$1s$-$2p_+$	-2.86[-3] 7.97[-4]	-2.83[-3] 1.14[-3]	-2.53[-3] 7.55[-4]	-2.77[-3] 1.73[-3]
	1	$1s$-$1s$	-7.01[-3]-3.70[-3]	-7.03[-3]-3.70[-3]	-7.06[-3]-3.68[-3]	
		$1s$-$2s$	1.72[-3] 2.03[-3]	1.62[-3] 1.96[-3]	1.60[-3] 2.04[-3]	1.16[-3] 2.02[-3]
		$1s$-$2p_-$	1.82[-2] 5.43[-3]	1.81[-2] 5.54[-3]	1.81[-2] 5.63[-3]	1.85[-2] 5.56[-3]
		$1s$-$2p_+$	-1.64[-3]-1.20[-3]	-1.64[-3]-1.18[-3]	-1.63[-3]-1.16[-3]	-1.29[-3]-1.02[-3]
		σ_{1s}	5.33[0]	5.37[0]	5.33[0]	
		σ_{2s}	2.48[-1]	2.50[-1]	2.52[-1]	2.58[-1]
		σ_{2p}	2.26[0]	2.27[0]	2.23[0]	2.06[0]
		σ_t	1.07[1]	1.08[1]	1.07[1]	

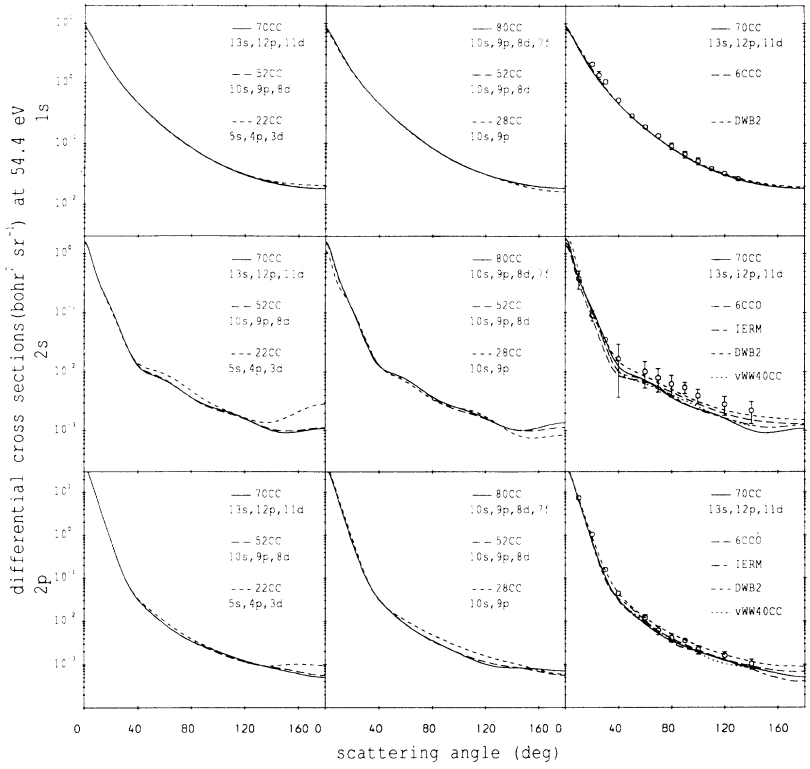

FIG. 4. Differential cross sections at 54.4 eV for the $1s$, $2s$, and $2p$ channels calculated with the indicated number of Laguerre basis states. The calculation of van Wyngaarden and Walters [24] is denoted by vWW40CC. See Fig. 1 for more detail and definition of other theories. The measurements for the elastic channel have been interpolated from Williams [27], and for the inelastic channels are due to Williams [28].

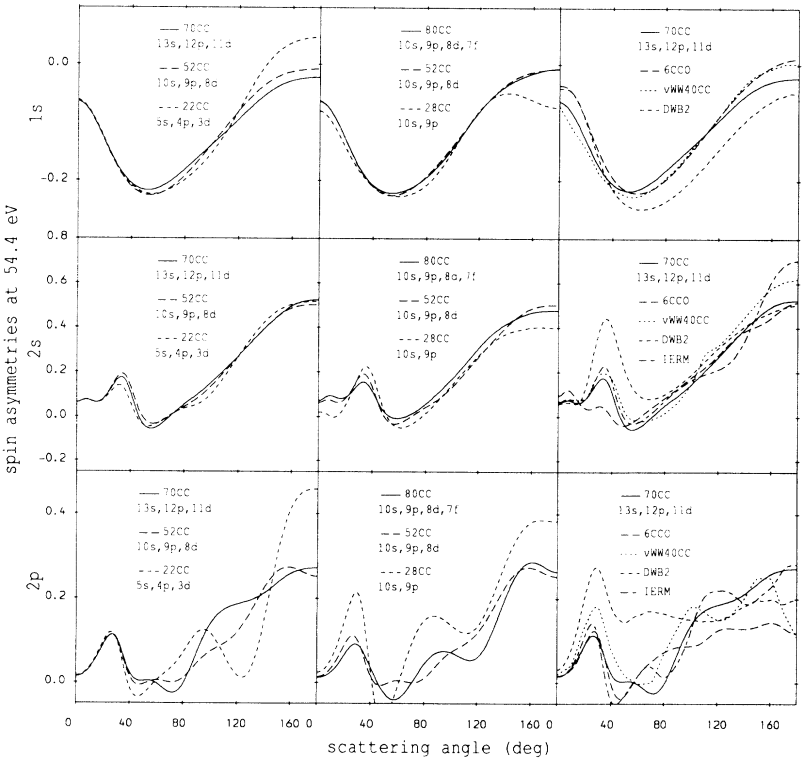

FIG. 5. Spin asymmetries at 54.4 eV for the $1s$, $2s$, and $2p$ channels calculated with the indicated number of Laguerre basis states. The calculation of van Wyngaarden and Walters [29, 30] is denoted by vWW40CC. See Fig. 1 for more detail and definition of other theories.

lations are significantly different then comparison with the 52CC elements gives an indication as to whether the lack of convergence is due to insufficient N_l or l_{max}. We see that, in general, agreement between the theories is very good; however, on occasion the IERM differs significantly from the others, which are in good agreement with each other. The IERM method involves matching outside the interaction region, uses T-matrix averaging, and includes corrections based on the plane-wave second-order Born approximation to make allowance for configurations not included in the IERM expansion of the three-body scattering wave function. As our method has no such approximations we suggest this is a possible source for the discrepancies.

The differential cross sections for the $1s$, $2s$, and $2p$ channels for electron hydrogen scattering at 54.4 eV are given in Fig. 4. Convergence is clearly demonstrated. Agreement with experiment and other theories is quite good, though our results are systematically a little lower than the measurements. At this energy as well as at 100 eV there is a large pseudostate calculation of van Wyngaarden and Walters [24]. This is a 40CC calculation with $N_l = 8$ and $l_{max} = 2$, where they also tried to take care of higher l by employing a distorted-wave second-order Born approximation. They used Slater-type orbitals for their basis which was chosen to get good second-order Born terms. We denote their results by vWW40CC.

The corresponding asymmetries are given in Fig. 5. Here we see that while convergence for the $1s$ and $2s$ channels is evident at all angles, it is not so clear for the $2p$ channel. Clearly larger calculations are necessary to establish convergence at all angles for the asymmetry of the $2p$ channel. Agreement with other theories is rather mixed with the DWB2 calculation standing out most from the others.

The 54.4-eV angular correlation parameters are given in Fig. 6. Very good convergence is evident at all angles for each parameter. Agreement with experiment, two independent sets of measurements, is very good at forward angles, but poor at intermediate angles for λ, and backward angles for the R parameter. The different theories tend to support each other, as do the two sets of measurements. The agreement with the measurements of the I parameter is also particularly disappointing since there is very good agreement between the various theories. Having established convergent close-coupling results we are forced to claim that the close-coupling theory is unable to explain the existing measurements of the angular correlation parameters.

Again it is instructive to look at the T-matrix elements given in Table II together with the integrated and total cross sections. We see that agreement between the 70CC, 80CC, and IERM theories is generally very good, though there are some significant differences on occasion. Given the nature of the agreement of the T matrices we were puzzled by the oscillations at backward angles of the IERM λ and R parameters. Since IERM is a hybrid theory which uses partial-wave T-matrix elements for $J \geq 5$ from an entirely separate pseudostate calculation, we calculated the angular correlation parameters for the IERM method using the T-matrix elements for $J \geq 5$ from our 70CC calculation. The resulting λ and R were free of the oscillations at the backward angles, but otherwise very

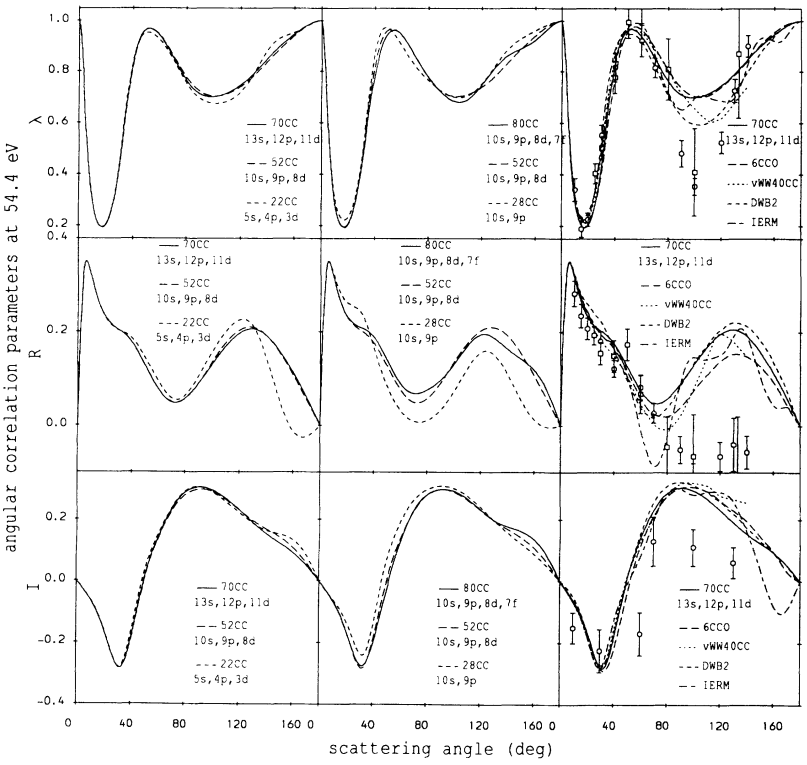

FIG. 6. Angular correlation parameters for the $2p$ excitation of hydrogen at 54.4 eV calculated with the indicated number of Laguerre basis states. See Figs. 1 and 4 for definition of other theories and more detail. The measurements denoted by ○ are due to Williams [28,31], those denoted by □ are due to Weigold, Frost, and Nygaard [32].

similar to those presented. This confirmed our suspicion that the oscillations in the IERM results are likely to be due to numerical problems. The integrated cross sections show remarkable convergence, and are in excellent agreement with IERM, and good agreement with experiment.

In Fig. 7 we present the differential cross sections at 100 eV. Clearly our results have converged, and are in very good agreement with other theories. Agreement with the elastic measurements is a little disappointing as all of the models lie a little lower than the experiment, but are in complete agreement with each other.

The corresponding asymmetries are given in Fig. 8. As at 54.4 eV, the covergence for the $1s$ and $2s$ channels is obtained at all angles, whereas it has not been established for some angles of the $2p$ channel. Agreement with the 6CCO and vWW40CC results is quite good, but it is surprising to see a large discrepancy with the DWB2 calculations at this relatively high energy. Whenever there

TABLE II. T-matrix elements (real and imaginary parts) for the first five partial waves J, and integrated and total cross sections (a_0^2) at 54.4 eV. The numbers in brackets indicate powers of 10.

J	S	Channel	52CC	70CC	80CC	IERM
0	0	$1s$-$1s$	-5.56[-2]-6.11[-2]	-5.65[-2]-6.16[-2]	-5.59[-2]-6.12[-2]	
		$1s$-$2s$	-5.88[-4] 1.62[-2]	-1.33[-3] 1.55[-2]	-1.69[-3] 1.69[-2]	-2.00[-3] 1.54[-2]
		$1s$-$2p$	9.50[-3] 1.58[-2]	1.02[-2] 1.64[-2]	9.35[-3] 1.47[-2]	1.07[-2] 1.72[-2]
	1	$1s$-$1s$	-7.54[-2]-8.93[-2]	-7.54[-2]-8.94[-2]	-7.54[-2]-8.95[-2]	
		$1s$-$2s$	-5.79[-3] 7.85[-3]	-5.73[-3] 7.68[-3]	-5.96[-3] 7.85[-3]	-6.02[-3] 6.78[-3]
		$1s$-$2p$	3.91[-4] 1.32[-2]	3.46[-4] 1.32[-2]	2.98[-4] 1.30[-2]	-8.89[-5] 1.41[-2]
1	0	$1s$-$1s$	-2.33[-2]-1.72[-2]	-2.42[-2]-1.82[-2]	-2.39[-2]-1.73[-2]	
		$1s$-$2s$	1.30[-2] 1.20[-2]	1.28[-2] 1.16[-2]	1.30[-2] 1.21[-2]	1.24[-2] 1.16[-2]
		$1s$-$2p_-$	6.73[-3] 5.80[-3]	6.66[-3] 5.73[-3]	6.49[-3] 5.73[-3]	7.40[-3] 6.46[-3]
		$1s$-$2p_+$	6.71[-3] 1.01[-3]	6.93[-3] 1.32[-3]	6.53[-3] 5.25[-4]	7.39[-3] 1.33[-3]
	1	$1s$-$1s$	-5.08[-2]-2.19[-2]	-5.10[-2]-2.21[-2]	-5.09[-2]-2.19[-2]	
		$1s$-$2s$	5.31[-3] 1.04[-2]	5.24[-3] 1.05[-2]	5.27[-3] 1.04[-2]	4.80[-3] 1.01[-2]
		$1s$-$2p_-$	8.85[-4] 3.35[-3]	8.43[-4] 3.38[-3]	7.47[-4] 3.36[-3]	9.98[-4] 3.76[-3]
		$1s$-$2p_+$	4.89[-3] 3.86[-3]	4.92[-3] 3.93[-3]	4.78[-3] 3.60[-3]	5.27[-3] 4.48[-3]
2	0	$1s$-$1s$	-1.25[-2]-1.28[-2]	-1.21[-2]-1.29[-2]	-1.27[-2]-1.28[-2]	
		$1s$-$2s$	8.90[-3] 3.97[-3]	9.12[-3] 3.98[-3]	8.99[-3] 4.04[-3]	8.38[-3] 3.50[-3]
		$1s$-$2p_-$	1.39[-2] 5.89[-3]	1.42[-2] 5.90[-3]	1.38[-2] 5.91[-3]	1.52[-2] 6.02[-3]
		$1s$-$2p_+$	5.00[-4]-1.34[-3]	5.14[-4]-1.42[-3]	4.84[-4]-1.54[-3]	1.73[-3]-1.48[-3]
	1	$1s$-$1s$	-2.32[-2]-6.73[-3]	-2.33[-2]-6.77[-3]	-2.32[-2]-6.79[-3]	
		$1s$-$2s$	8.13[-3] 5.81[-3]	8.20[-3] 5.87[-3]	8.10[-3] 5.76[-3]	7.79[-3] 5.37[-3]
		$1s$-$2p_-$	6.30[-3] 6.70[-3]	6.25[-3] 6.67[-3]	6.17[-3] 6.73[-3]	6.71[-3] 6.96[-3]
		$1s$-$2p_+$	2.60[-3]-5.03[-4]	2.68[-3]-4.96[-4]	2.52[-3]-6.28[-4]	3.77[-3]-1.06[-4]
3	0	$1s$-$1s$	-8.42[-3]-8.92[-3]	-8.26[-3]-8.57[-3]	-8.35[-3]-8.87[-3]	
		$1s$-$2s$	4.50[-3] 2.62[-3]	4.61[-3] 2.73[-3]	4.68[-3] 2.58[-3]	4.03[-3] 2.51[-3]
		$1s$-$2p_-$	1.64[-2] 2.05[-3]	1.65[-2] 2.44[-3]	1.63[-2] 2.10[-3]	1.68[-2] 2.32[-3]
		$1s$-$2p_+$	-1.98[-3]-5.88[-4]	-1.90[-3]-6.49[-4]	-2.00[-3]-7.06[-4]	-1.49[-3]-4.53[-4]
	1	$1s$-$1s$	-1.10[-2]-4.37[-3]	-1.10[-2]-4.29[-3]	-1.10[-2]-4.32[-3]	
		$1s$-$2s$	6.17[-3] 2.58[-3]	6.10[-3] 2.66[-3]	6.19[-3] 2.60[-3]	5.43[-3] 2.35[-3]
		$1s$-$2p_-$	1.14[-2] 6.08[-3]	1.14[-2] 6.08[-3]	1.12[-2] 6.05[-3]	1.18[-2] 6.25[-3]
		$1s$-$2p_+$	7.75[-5]-1.39[-3]	8.46[-5]-1.37[-3]	2.31[-5]-1.45[-3]	5.85[-4]-1.19[-3]
4	0	$1s$-$1s$	-5.73[-3]-5.69[-3]	-5.82[-3]-5.57[-3]	-5.72[-3]-5.49[-3]	
		$1s$-$2s$	2.23[-3] 2.62[-3]	2.26[-3] 2.69[-3]	2.45[-3] 2.68[-3]	1.39[-3] 2.73[-3]
		$1s$-$2p_-$	1.56[-2]-2.17[-4]	1.54[-2]-9.73[-5]	1.56[-2] 3.07[-4]	1.57[-2]-2.66[-4]
		$1s$-$2p_+$	-2.83[-3] 1.17[-4]	-2.76[-3] 1.50[-4]	-2.52[-3] 1.50[-4]	-2.58[-3] 6.42[-4]
	1	$1s$-$1s$	-6.12[-3]-3.53[-3]	-6.14[-3]-3.51[-3]	-6.17[-3]-3.48[-3]	
		$1s$-$2s$	3.64[-3] 1.52[-3]	3.63[-3] 1.55[-3]	3.57[-3] 1.58[-3]	3.09[-3] 1.52[-3]
		$1s$-$2p_-$	1.35[-2] 3.73[-3]	1.34[-2] 3.71[-3]	1.35[-2] 3.85[-3]	1.39[-2] 4.02[-3]
		$1s$-$2p_+$	-1.42[-3]-1.05[-3]	-1.42[-3]-1.06[-3]	-1.41[-3]-1.02[-3]	-1.13[-3]-9.22[-4]
		σ_{1s}	3.01[0]	3.03[0]	3.02[0]	
		σ_{2s} 1.76(12)[-1][a]	2.08[-1]	2.08[-1]	2.12[-1]	2.07[-1]
		σ_{2p} 2.26(9)[0][a]	2.32[-1]	2.32[0]	2.26[0]	2.27[0]
		σ_t	8.58 [0]	8.56[0]	8.52[0]	

[a]The estimates of the $2s$ and $2p$ integrated cross sections are due to van Wyngaarden and Walters [24].

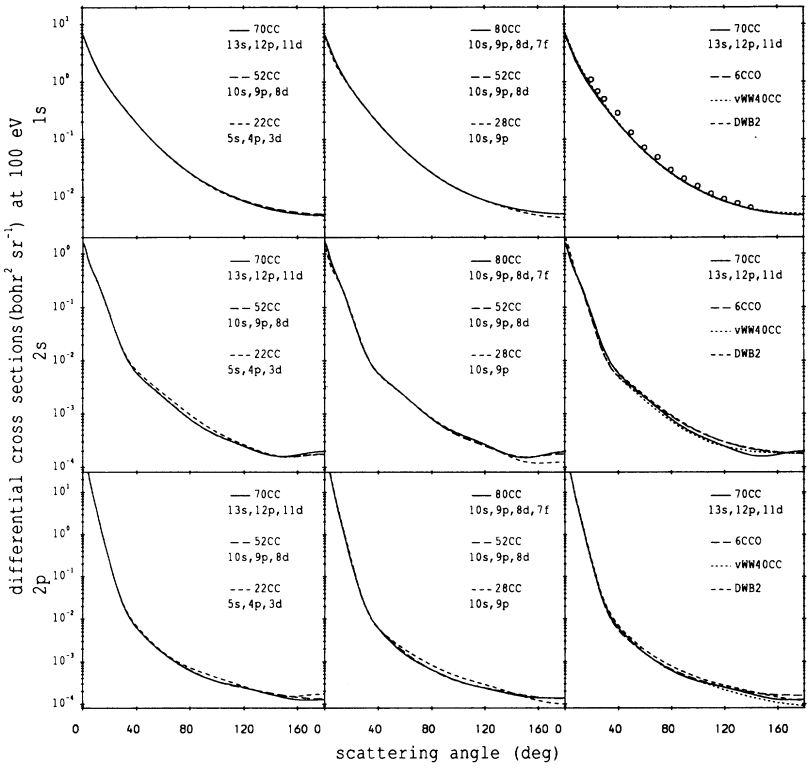

FIG. 7. Differential cross sections at 100 eV for the $1s$, $2s$, and $2p$ channels calculated with the indicated number of Laguerre basis states. See Figs. 1 and 4 for definition of other theories and more detail.

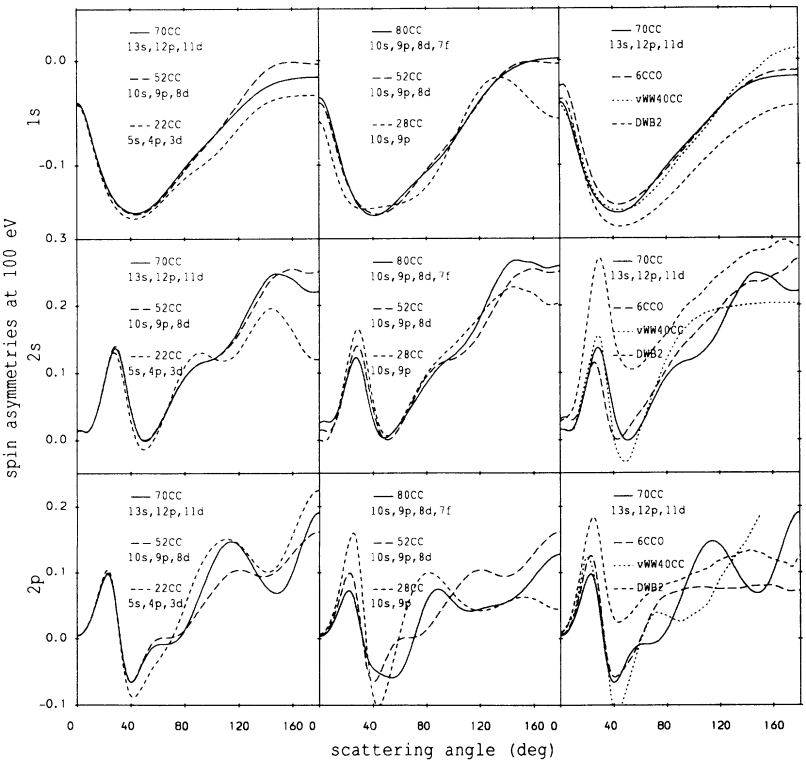

FIG. 8. Spin asymmetries at 100 eV for the $1s$, $2s$, and $2p$ channels calculated with the indicated number of Laguerre basis states. See Figs. 1 and 5 for definition of other theories and more detail.

is a problem with convergence it is instructive to look at the T-matrix elements which are given together with the integrated and total cross sections, which demonstrate excellent convergence, in Table III. Comparing 52CC and 70CC elements for the $1s$-$2p$ channel we see excellent agreement from which we would have expected almost indistinguishable asymmetries. To find the cause of the problem we replaced just the $J = 0$ T-matrix elements of the 52CC calculation with those of the 70CC calculation, i.e., a change of at most 1%. We found that the resultant asymmetry varied from the 52CC by as much as 10% at the backward angles. As the differential cross

TABLE III. T-matrix elements (real and imaginary parts) for the first five partial waves J, and integrated and total cross sections (a_0^2) at 100 eV. The numbers in brackets indicate powers of 10.

J	S	Channel	52CC	70CC	80CC
0	0	$1s$-$1s$	-4.40[-2]-3.89[-2]	-4.43[-2]-3.85[-2]	-4.40[-2]-3.91[-2]
		$1s$-$2s$	2.75[-3] 9.97[-3]	2.69[-3] 9.92[-3]	2.44[-3] 1.00[-2]
		$1s$-$2p$	5.21[-3] 7.30[-3]	5.22[-3] 7.33[-3]	5.34[-3] 6.69[-3]
	1	$1s$-$1s$	-5.47[-2]-4.74[-2]	-5.48[-2]-4.72[-2]	-5.47[-2]-4.74[-2]
		$1s$-$2s$	-6.74[-4] 7.47[-3]	-5.83[-4] 7.34[-3]	-7.45[-4] 7.49[-3]
		$1s$-$2p$	2.50[-3] 7.16[-3]	2.51[-3] 7.09[-3]	2.61[-3] 7.01[-3]
1	0	$1s$-$1s$	-2.23[-2]-1.22[-2]	-2.25[-2]-1.25[-2]	-2.25[-2]-1.23[-2]
		$1s$-$2s$	8.27[-3] 6.55[-3]	8.21[-3] 6.53[-3]	8.22[-3] 6.60[-3]
		$1s$-$2p_-$	2.78[-3] 2.43[-3]	2.79[-3] 2.44[-3]	2.83[-3] 2.32[-3]
		$1s$-$2p_+$	3.06[-3] 1.09[-3]	3.03[-3] 1.07[-3]	3.12[-3] 8.57[-4]
	1	$1s$-$1s$	-3.38[-2]-1.32[-2]	-3.39[-2]-1.34[-2]	-3.38[-2]-1.33[-2]
		$1s$-$2s$	4.86[-3] 6.24[-3]	4.85[-3] 6.29[-3]	4.85[-3] 6.28[-3]
		$1s$-$2p_-$	1.09[-3] 2.16[-3]	1.10[-3] 2.19[-3]	1.11[-3] 2.10[-3]
		$1s$-$2p_+$	2.68[-3] 1.86[-3]	2.64[-3] 1.84[-3]	2.70[-3] 1.75[-3]
2	0	$1s$-$1s$	-1.15[-2]-7.87[-3]	-1.18[-2]-7.83[-3]	-1.17[-2]-7.84[-3]
		$1s$-$2s$	7.25[-3] 2.84[-3]	7.20[-3] 2.95[-3]	7.26[-3] 2.97[-3]
		$1s$-$2p_-$	6.40[-3] 2.73[-3]	6.32[-3] 2.67[-3]	6.30[-3] 2.60[-3]
		$1s$-$2p_+$	6.51[-4]-3.41[-4]	5.75[-4]-3.98[-4]	5.44[-4]-4.78[-4]
	1	$1s$-$1s$	-1.78[-2]-5.16[-3]	-1.80[-2]-5.21[-3]	-1.78[-2]-5.17[-3]
		$1s$-$2s$	5.94[-3] 3.72[-3]	5.92[-3] 3.75[-3]	5.97[-3] 3.77[-3]
		$1s$-$2p_-$	4.04[-3] 3.27[-3]	3.98[-3] 3.23[-3]	4.03[-3] 3.20[-3]
		$1s$-$2p_+$	1.31[-3]-3.01[-5]	1.26[-3]-4.79[-5]	1.22[-3]-1.30[-4]
3	0	$1s$-$1s$	-6.63[-3]-5.75[-3]	-6.60[-3]-5.73[-3]	-6.73[-3]-5.71[-3]
		$1s$-$2s$	5.30[-3] 1.53[-3]	5.30[-3] 1.54[-3]	5.35[-3] 1.62[-3]
		$1s$-$2p_-$	8.48[-3] 1.70[-3]	8.43[-3] 1.76[-3]	8.30[-3] 1.59[-3]
		$1s$-$2p_+$	-8.29[-4]-4.28[-4]	-8.33[-4]-3.85[-4]	-8.83[-4]-4.66[-4]
	1	$1s$-$1s$	-9.50[-3]-3.19[-3]	-9.51[-3]-3.17[-3]	-9.52[-3]-3.17[-3]
		$1s$-$2s$	5.21[-3] 2.04[-3]	5.21[-3] 2.04[-3]	5.23[-3] 2.08[-3]
		$1s$-$2p_-$	6.43[-3] 2.96[-3]	6.39[-3] 2.97[-3]	6.34[-3] 2.87[-3]
		$1s$-$2p_+$	6.09[-6]-5.78[-4]	5.87[-6]-5.69[-4]	-6.20[-5]-6.22[-4]
4	0	$1s$-$1s$	-4.13[-3]-4.28[-3]	-4.18[-3]-4.28[-3]	-4.28[-3]-4.21[-3]
		$1s$-$2s$	3.58[-3] 1.09[-3]	3.56[-3] 1.15[-3]	3.69[-3] 1.22[-3]
		$1s$-$2p_-$	9.28[-3] 7.37[-4]	9.27[-3] 6.97[-4]	9.00[-3] 7.24[-4]
		$1s$-$2p_+$	-1.72[-3]-2.49[-4]	-1.68[-3]-2.44[-4]	-1.63[-3]-1.68[-4]
	1	$1s$-$1s$	-5.36[-3]-2.58[-3]	-5.38[-3]-2.58[-3]	-5.41[-3]-2.56[-3]
		$1s$-$2s$	3.95[-3] 1.16[-3]	3.93[-3] 1.18[-3]	3.98[-3] 1.22[-3]
		$1s$-$2p_-$	7.86[-3] 2.16[-3]	7.87[-3] 2.14[-3]	7.73[-3] 2.08[-3]
		$1s$-$2p_+$	-9.40[-4]-6.01[-4]	-9.42[-4]-5.95[-4]	-9.54[-4]-5.95[-4]
		σ_{1s} 1.85[0][a]	1.40[0]	1.41[0]	1.41[0]
		σ_{2s} 1.22(13)[-1][b]	1.39[-1]	1.39[-1]	1.40[-1]
		σ_{2p} 1.94(9)[0][b]	1.98[0]	1.98[0]	1.96[0]
		σ_t 6.84[0][a]	6.11[0]	6.11[0]	6.15[0]

[a]The semiempirical estimates of the integrated elastic and total cross section are due to de Heer, McDowell, and Wagenaan [25].

[b]The estimates of the $2s$ and $2p$ integrated cross sections are due to van Wyngaarden and Walters [24].

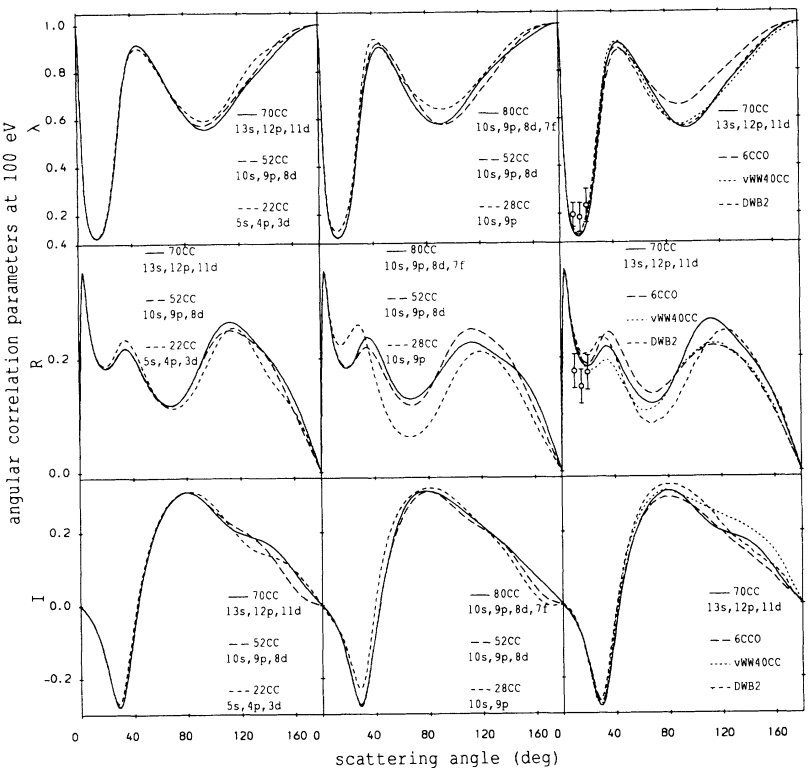

FIG. 9. Angular correlation parameters for the $2p$ excitation of hydrogen at 100 eV calculated with the indicated number of Laguerre basis states. See Figs. 1 and 4 for definition of other theories and more detail. The measurements are due to Hood, Weigold, and Dixon [33].

section at the backward angles is so small for the larger energies a small variation in the lowest partial waves has a large effect on the backward angles of the asymmetry parameter. This explains the large variation between the various theories at the these angles.

Looking at the integrated and total cross sections we see excellent convergence. Agreement with experiment is not very good for the elastic and total cross sections. Our integrated elastic cross section is around 20% lower than experiment. This follows from the fact that our elastic differential cross section is lower than experiment by about the same amount (see Fig. 7). As the experimental total-cross-section determination uses this elastic cross section it is not surprising to see our result for total cross section is also considerably lower than the experimental estimate. Agreement with the experimental estimates of the $2s$ and $2p$ integrated cross sections is very good.

Finally, we look at the 100-eV angular correlation parameters in Fig. 9. We see that convergence has been established and agreement with other theories and the few available measurements is quite good. These measurements are only at the forward angles, and so should be reproduced by most theories, since this region is dominated mainly by the high partial waves which are essentially given by the first-order Born approximation.

In addition to the calculations reported, we carried out many more calculations in order to test the convergence rates for the amplitudes. Additional tests, for example, were to calculate the T-matrix amplitudes by varying N_l in integer steps up to the maximum sizes discussed in this section. The results selected for presentation are indicative of the general trend of convergence we obtained in these studies.

V. CONCLUSIONS

Our aim in this paper has been to develop a framework for the solution of the close-coupling equations using L^2 expansions for the hydrogen atom target, which can be increased to arbitrary basis size, hence enabling overall convergence of the scattering amplitudes to be studied systematically. The methods developed are numerically stable and our calculations have been limited only by the local computing facilities available.

We have established convergent differential, integrated, and total cross sections for elastic scattering and inelastic scattering to the $2s$ and $2p$ levels over a range of energies 35, 54.4, and 100 eV. As there is very little difference between our 70CC and 52CC calculations at all energies for the differential cross sections, convergence is obtained by having $13s$, $12p$, and $11d$ states in the expansions. We tested the effect of f states in the target expansion by adding $7f$ states to our 52CC calculation. Since their effect is minimal, it is our opinion that the cross sections presented will not be significantly changed by more extensive basis sets. We have reached the point where close coupling is complete.

Angular correlations provided a more stringent test of the phase and magnitude of the scattering amplitude to the $2p$ level. By restricting the basis to s, p, and d states and extending its size we obtained convergent λ, R, and I correlations. Inclusion of f states results in up to a 10% change in their values at some large scattering angles.

So if higher precision was required at these angles then perhaps even higher l states would be required. All our calculations are unable to reproduce the deep minima at backward angles in λ for the 35- and 54.4-eV experiments and there is a similar divergence in the R parameter with the 54.4-eV experiments. While we are unable to claim convergence to a 1% level, it does appear that our correlations will not be altered substantially by more extended calculations, certainly not sufficiently to explain the discrepancy with experiment.

Spin asymmetries proved to be the most sensitive parameters to target basis sets. For basis sets restricted to s, p, and d states, convergence with basis is achieved to within a few percent over most of the angular range. The elastic channel asymmetry has a single minimum and rises at backward angles. Discrepancies of up to 10% were obtained in the 100-eV result for angles greater than 120°. The $2s$ spin asymmetries have a node at forward angles which is followed by a steady rise at backward angles. Convergence rates are similar to the $1s$ channel. The $2p$ channel shows most structure. The calculations over s, p, and d basis states indicate a well-defined forward peak and subsequent nodal structure that is similar for the 52CC and 70CC models. The main differences are again at extreme backward angles where the cross section is very small. When f states are added to the 52CC model, their effect is significant in altering the magnitude of the forward peak of the $2p$ channel but not its position, and in addition varies the shape and structure of the remaining peaks. The convergence was reasonably demonstrated for the 35-eV results but becomes progressively worse at 54.4 and 100 eV. We conclude that states of higher partial waves are needed at 54.4 and 100 eV in order to obtain better convergence for the $2p$ channel spin asymmetry.

At this stage, where our results and experiment disagree we have good agreement with other theories, the nonperturbative IERM of Scholz *et al.*, vWW40CC of van Wyngaarden and Walters, CCO of Bray and coworkers and the perturbative (exact to second order) DWB2 of Madison, Bray, and McCarthy. Where there is significant discrepancy between the theories, particularly the asymmetries, there is no experiment. It would be most helpful if new measurements of the angular correlation parameters as well as measurements of the hydrogen asymmetries were available. Given the excellent quantitative agreement in electron-sodium scattering measurements of the $L_\perp = -2\sqrt{2}I$ parameter and the CCO theory of Bray and McCarthy [21], which is an approximation to the convergent CC theory pesented here, we are not too perturbed by the present discrepancies between theory and experiment in electron-hydrogen scattering.

Our overall conclusion is that the Laguerre basis expansions applied here are adequate to obtain fully convergent scattering amplitudes in the close-coupling equations. In the calculations reported, we have demonstrated convergence of individual partial-wave T-matrix amplitudes for channels of interest to better than 5% level over all the energy range considered with few exceptions. For parameters which are made from the summed partial waves we achieve convergence in some cases to better than 2%. We have demonstrated this for differential cross sections and to a lesser extent the angular correlations. Larger basis expansions are needed to obtain convergent spin asymmetries at all angles and energies to better than 10%. Achieving significantly better convergence for the amplitudes, say to a 1% level, is likely to require a large scaling up of our present calculations based on our experience [11] with the Poet model which required 30 $l = 0$ states. Extrapolating to our current models, it is reasonable to suggest that a 200CC calculation could be required, which is well within the capacity of modern supercomputers.

ACKNOWLEDGMENTS

We thank Professor Ian McCarthy for many useful discussions. We would also like to acknowledge support from the Australian Research Council.

* Electronic address: igor@esm.cc.flinders.edu.au
† Electronic address: stelbovi@atsibm.csu.murdoch.edu.au

[1] P.G. Burke and T.G. Webb, J. Phys. B **3**, L131 (1970).
[2] P.G. Burke and J.F. Mitchell, J. Phys. B **6**, 320 (1973).
[3] E.J. Heller, W.P. Reinhardt, and H.A. Yamani, J. Comput. Phys. **13**, 536 (1973).
[4] H.A. Yamani and W.P. Reinhardt, Phys. Rev. A **11**, 1144 (1975).
[5] A.T. Stelbovics and T. Winata, Aust. J. Phys. **43**, 485 (1990).
[6] R. Poet, J. Phys. B **11**, 3081 (1978).
[7] R. Poet, J. Phys. B **14**, 91 (1981).
[8] D.H. Oza and J. Callaway, Phys. Rev. A **27**, 2840 (1983).
[9] D.H. Oza, Phys. Rev. A **30**, 1101 (1984).
[10] E.J. Heller and H.A. Yamani, Phys. Rev. A **9**, 1209 (1974).
[11] I. Bray and A.T. Stelbovics, Phys. Rev. Lett. **69**, 53 (1992).
[12] I.E. McCarthy and A.T. Stelbovics, Phys. Rev. A **28**, 2693 (1983).
[13] I.C. Percival and M.J. Seaton, Proc. Cambridge Philos. Soc. **53**, 654 (1957).
[14] A.T. Stelbovics, Phys. Rev. A **41**, 2536 (1990).
[15] I. Bray, D. A. Konovalov, and I. E. McCarthy, Phys. Rev. A **43**, 1301 (1991).
[16] E. Bank and M. Ismail, Constr. Approx. **1**, 103 (1985).
[17] A.T. Stelbovics, J. Phys. B **22**, L159 (1989).
[18] E. Anderson, Z. Bai, C. Bischof, J. Demmel, J. Dongarra, J. Du Croz, A. Greenbaum, S. Hammarling, A. McKenney, S. Ostroucnov, and D. Sorensen, LAPACK *User's Guide* (Society for Industrial and Applied Mathematics, Philadelphia, PA, 1992).
[19] I. Bray, D.A. Konovalov, and I.E. McCarthy, Phys. Rev. A **44**, 5586 (1991).
[20] Nils Andersen, Jean W. Gallagher, and Ingolf V. Hertel, Phys. Rep. **165**, 1 (1988).
[21] I. Bray and I.E. McCarthy, Phys. Rev. A (to be published).
[22] T.T. Scholz, H.R.J. Walters, P.G. Burke, and M.P. Scott, J. Phys. B **24**, 2097 (1991).

[23] D.H. Madison, I. Bray, and I.E. McCarthy, J. Phys. B **24**, 3861 (1991).
[24] W.L. van Wyngaarden and H.R.J. Walters, J. Phys. B **19**, 929 (1986).
[25] F.J. de Heer, M.R.C. McDowell, and R.W. Wagenaar, J. Phys. B **10**, 1945 (1977).
[26] J. Slevin, M. Eminyan, J.M. Woolsey, G. Vassilev, H. Q. Porter, C.G. Back, and S. Watkin, Phys. Rev. A **26** 1344 (1982).
[27] J.F. Williams, J. Phys. B **8**, 2191 (1975).
[28] J.F. Williams, J. Phys. B **14**, 1197 (1981).
[29] W.L. van Wyngaarden and H.R.J. Walters, J. Phys. B **19**, 1817 (1986).
[30] W.L. van Wyngaarden and H.R.J. Walters, J. Phys. B **19**, 1827 (1986).
[31] J.F. Williams, Aust. J. Phys. **39**, 621 (1986).
[32] E. Weigold, L. Frost, and K.J. Nygaard, Phys. Rev. A **21**, 1950 (1979).
[33] S.T. Hood, E. Weigold, and A J. Dixon, J. Phys. B **12**, 631 (1979).